International Journal of Thermofluid Science and Technology (2019)
Volume 6, Issue 2, Paper No. 19060202
https://doi.org/10.36963/IJTST.19060202

Research Article

HHR impact on 3D radiative stretched flow of Cu-H_2O nanofluid influenced by variable magnetic field and convective boundary condition

M. K. Nayak

Department of Physics, IHSE, Siksha 'O' Anusandhan Deemed to be University, Bhubaneswar-751003, Odisha, India

Received: 11 June 2019; Received in revised form: 8 October 2019; Accepted: 18 October 2019;
Published online: 10 November 2019

Abstract

In an attempt to the influence of homogenous and heterogeneous reactions, variable magnetic field and thermal radiation on three-dimensional flow of an incompressible nanofluid over an exponential stretching sheet subject to convective boundary condition has been analyzed. In view of enhancement of heat transfer capability of nanofluids, effective implementation of Patel model is carried in the current study. The transformed governing differential equations are solved using fourth-order Runge-Kutta method along with shooting technique and secant method is employed for better approximation. The significant outcome of the present computational study is that the magnetic field interaction impedes the fluid motion leading to diminution of the wall shear stresses (axial as well as transverse) and homogenous and heterogeneous parameters belittle the fluid concentration appreciably.

Keywords: MHD 3D flow; Nanofluid; Exponential stretching sheet; Convective boundary condition; Thermal radiation; Homogenous and heterogeneous reactions (HHR).

1. Introduction

The claims of advanced science and technology in the recent world are based on the principle of reproducibility of results. There's been a modest surge in keeping young researchers seeking investigation regarding the several aspects of flow and heat transfer of nanofluids over various types of surfaces. This is because of massive significant engineering applications of nanofluids such as better and safer coolant in nuclear reactors, cancer therapy, heat exchangers, micro-channel heat sinks and several electronic devices for military sectors, vehicles and transformers, the waste heat removal equipment design and manufacturing of materials and chemicals.

Ironically, nanofluids are fluids that possess nanoparticles viz. metals, oxides, carbides, nitrides and carbon nanotubes (particles of 100nm or less size) along with many conventional

Corresponding email: mkn2122@gmail.com

fluids (base fluids) such as water, kerosene, engine oil, touline, ethylene glycol and tri-ethylene glycol etc.

Nomenclature

(u,v,w)	velocity components in (x, y,z) directions (ms^{-1})		
$\left(k_{nf},k_f,k_s\right)$	thermal conductivities of (nanofluid, base fluid, nanoparticle) ($Wm^{-1}K^{-1}$)		
$\left(\mu_{nf},\mu_f\right)$	effective viscosity of (nanofluid, base fluid)		
$\left(\sigma_{nf},\sigma_f\right)$	effective viscosity of (nanofluid, base fluid)		
(Γ,Γ_1)	Homogeneous and heterogeneous reaction rates		
(U_0,V_0,U_w,V_w,c)	constants		
$\left(C_{fx},C_{fy}\right)$	skin frictions		
$\left(\rho C_p\right)_f$	heat capacitance of base fluid ($Jm^{-3}K^{-1}$)		
ϕ	solid volume fraction		
$\left(F(\eta),G(\eta)\right)$	dimensionless stream functions	$\left(\rho C_p\right)_s$	heat capacitance ($Jm^{-3}K^{-1}$)
υ_f	dynamic viscosity$\left(m^2s^{-1}\right)$	$\left(Re_x,Re_y\right)$	local Reynolds number
T	temperature of fluid (K)	T_∞	Ambient fluid temperature (K)
T_w	surfacetemperature (K)	T_f	surfacetemperature (K)
L	reference length (m)	j_0	current density (A/m^2)
B_0	uniform magnetic field strength	σ^*	Stefan Boltzmann constant($Wm^{-2}K^{-4}$)
k^*	mean absorption coefficient	ρ_{nf}	effective density of nanofluid(kgm^{-3})
$\left(\rho C_p\right)_{nf}$	heat capacitance of nanofluid($Jm^{-3}K^{-1}$)	ρ_f	density of base fluid (kgm^{-3})
$\left(\mathrm{Re}_x,\mathrm{Re}_y\right)$	local Reynolds numbers	$\left(\tau_{wx},\tau_{wy}\right)$	wall shear stresses
ρ_s	density of nanoparticles (kgm^{-3})	μ_{nf}	dynamic viscosity (NSm^{-2})
μ_f	dynamic viscosity of base fluid (NSm^{-2})	η	non-dimensional vertical distance
M	Hartmann number	h_f	heat transfer coefficient
P_r	Prandtl number	Rd	radiation parameter
Sc	Schmidt number	Bi	Biot's number
q_w	wall heat flux	Ω	ratio of diffusion coefficients

Subscripts

nf	nanofluid	p	*particle*
f	fluid	s	surface
w	quantities at wall	∞	quantities at free stream

Greek Symbols

ϕ,η,ρ_f,σ

All because of the enhancement of the thermal conductivity and hence heat transfer capabilities of nanofluids (due to use of additives), these are served as best suitable coolants in the above mentioned applications. Choi, 1995 discovered first the enhancement of thermal conductivity of nanofluids. The contribution of Khan and Pop, 2010 to the boundary layer flow of nanofluids over stretching surfaces can never be sidelined. Later, Makinde and Aziz, 2011 implemented the convective boundary condition in exhibiting boundary-layer flow of a nanofluid over a stretching surface. Many other researchers (Sheikholeslami & Shehzad, 2017; Sheikholeslami et al., 2017; Pandey & Kumar, 2017; Alsabery et al., 2016; Reddy & Chamkha, 2016; Nayak et al., 2017 and Prasad et al., 2018) have been working for further development in this area.

What is important to note is that the vital and inevitable applications of MHD nanofluid flow and heat transfer include wound treatment, gastric medications , targeted drug release, asthma treatment, cancer therapy, magnetic cell separation, sterilized equipments, magnetic resonance imaging, hyperthermia for tumor extraction etc. On account of such significant applications many researchers have been motivated to study in the related areas. The effect of external magnetic source on the flow of $Fe_3O_4 - H_2O$ nanofluid in a porous cavity has been declared by Sheikholeslami and Shehzad, 2018. The impact of inclined magnetic field associated with partial slip and constant heat flux undergoing mixed convection in a cavity with a nanofluid is studied by Ismael et al., 2016. The influence of partial slip and Joule heating on MHD peristaltic flow of hyperbolic tangent nanofluid wherein larger values of Hartman number enhance the fluid temperature has been observed by Hayat et al., 2016. In the hoary past, Makinde and Animasaun, 2016 have studied MHD bio-convection flow of nanofluid over an upper surface of a paraboloid of revolution. In their investigation they revealed that at fixed magnetic parameter, the local skin friction becomes more at large thickness parameter whereas local heat transfer rate becomes less at small temperature parameter.

What is clear, however, is that the convective boundary condition enhances the temperature and therefore the thermal conductivity of the nanofluids. This is why it is inevitable to consider the convective boundary condition as is more suitable model compared to isothermal conditions. Nayak, 2017 discussed the effect of convective boundary conditions in a radiating nanofluid flow subject to viscous dissipation. Further, Nayak et al. 2017 investigated the influence of convective boundary conditions on three dimensional flow of nanofluid over an exponential stretching sheet in presence of variable magnetic field. More recently, Gupta et al., 2018 discussed convective stagnation point radiative flow and heat transfer of nanofluid associated with chemical reaction. Interestingly, the impact of double stratification, viscous dissipation and Joule heating on magnetohydrodynamic convective flow of nanofluid was studied in Daniel et al., 2017.

There is a dire need for the knowing of the facts regarding thermal radiation effect which is felt to be important in the situations with large temperature gap between the boundary surface and ambient fluid. Also such effect is used to obtain high thermal efficiency from devices operating at high temperature levels for space applications. For these reasons, the radiation effects are essentially used in the design of many advanced conversion systems. Makinde and Ogulu, 2008 found by investigating that increase in thermal radiation enhances the non-dimensional temperature profiles in a flow of a variable viscosity fluid over a vertical porous plate in presence of transverse magnetic field. Nayak, 2016 analyzed in his study that stronger thermal radiation imparts more cooling associated with MHD viscoelastic fluid flow over a stretching sheet. The

effect of thermal radiation as well as viscous dissipation in response to chemical reaction was reported by Mabood et al., 2016. In their investigation it is described that thermal radiation significantly influences the temperature distributions of nanofluids in the manner that thermal radiation increases the thermal diffusion thereby increasing the fluid temperature irrespective of nature of nanoparticles. Very recently, Khan et al., 2017, Khan et al., 2017, Khan and khan, 2016 and Sohail et al., 2017 studied the effects of non-linear themal radiation, melting heat transfer, thermophoresis particle deposition on MHD flow of Burger fluid considering gyrotactic microorganisms as the nanoparticles. Many others (Nayak et al., 2018, Nayak et al., 2018, Priyadarsan et al., 2017) also put their efforts to explore the influence of thermal radiation along with velocity slip and internal heating on flow of different nanofluids over different surfaces under different situations.

It would be much more remarkable to bring focus the effective implementation of chemical reaction on diversified fields such as pollution studies, oxidation and synthesis materials, polymer production and fibrous insulation, the design of chemical processing equipment, processing of food, cooling towers, formation and dispersion of fog, temperature and moisture distribution over agricultural fields, damage of crops due to freezing etc. In fact this is such a common sight where the molecular dispersal of species due to chemical reaction cannot be ignored. In several systems such as catalysis, biochemical systems and combustion, chemical reactions involve homogeneous and heterogeneous reactions. Such reactions represent consumption and production of reactant species with different rates. The effect of heterogeneous-homogenous processes on MHD flow of Burger fluid on three dimensional surfaces was studied by Khan et al., 2016. Further, Nayak et al. and 2014, Nayak et al., 2017, Nayak et al., 2018 and Sengupta and Deb, 2018 studied in the related areas.

According to above literature studies, an investigation has yet to be made on the influence of homogenous and heterogeneous reactions on three-dimensional nanofluid flow past an exponentially-stretching sheet with a convective boundary condition subject to variable magnetic field and thermal radiation employing Patel model (Patel et al., 2005).

The objective of our study is to focus on the impact of homogenous and heterogeneous reactions, variable magnetic field and thermal radiation in 3D nanofluid flows over an exponentially-stretching sheet using a convective boundary condition.

The novelty of the present study in 3D exponential stretched flow includes:

- Homogenous and heterogeneous reactions are taken into account.
- Exponentially variable magnetic field is introduced.
- Thermal radiation effect is taken into consideration.

It is good that in the presented analysis, the similarity transformed governing boundary layer equations are solved numerically by using the fourth-order Runge-Kutta method along with the shooting technique. Furtermore, Secant method is implemented for good approximation. The influence ofseveral pertinent physical parameters of interest on the dimensionless velocity, temperature and concentration along with the skin friction and the local Nusselt number has been explored through appropriate graphs and tables.

2. Formulation of the problem

In the present we consider a steady three-dimensional boundary layer flow of an electrically-conducting magnetohydrodynamic $Cu-H_2O$ nanofluid over an exponentially-stretching sheet as shown in Fig.1. Assume that (1) the flow is steady, laminar and incompressible (2) variable thermal conductivity is implemented (3) gravitational effect is negligible, (4) convective boundary condition representing heat transfer rate through the surface is introduced, (5) a variable magnetic field $B=B_0 e^{\frac{x+y}{2L}}$ is introduced in the flow, (6) heterogeneous and homogeneous reactions are taken into considerations and (7) the induced magnetic field and the electric field are negligible.

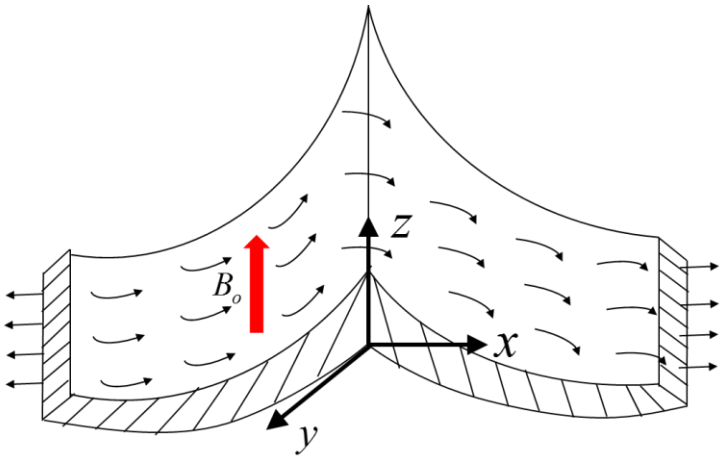

Fig.1 Flow geometry of the problem.

In respect of cubic autocatalysis, the homogenous reaction is defined mathematically as

$$A+2B\rightarrow 3B, rate=k_1^* a_1 b_1^2$$

While the first order isothermal reaction on the surface of the catalyst is

$$A\rightarrow B, rate=k_2^* a_1$$

Where a_1 and b_1 stand for the concentration of chemical species A and B respectively and $\left(k_1^*, k_2^*\right)$ are the rate of chemical species constants. It is a fact that such reactions are isothermal and in the ambient fluid, the reactant A possesses a consistent concentration a_0 and B is the non-auto catalyst.

Considering the aforementioned assumptions, the steady boundary layer governing equations indicating conservation of mass, momentum, energy and concentration are (Hayat et al., 2016, Nayak et al., 2018):

$$\frac{\partial u}{\partial x}+\frac{\partial v}{\partial y}+\frac{\partial w}{\partial z}=0 \tag{1}$$

$$u\frac{\partial u}{\partial x}+v\frac{\partial u}{\partial y}+w\frac{\partial u}{\partial z}=\frac{\mu_{nf}}{\rho_{nf}}\frac{\partial^2 u}{\partial z^2}-\frac{\sigma_{nf}B^2 u}{\rho_{nf}} \tag{2}$$

$$u\frac{\partial v}{\partial x}+v\frac{\partial v}{\partial y}+w\frac{\partial v}{\partial z}=\frac{\mu_{nf}}{\rho_{nf}}\frac{\partial^2 v}{\partial z^2}-\frac{\sigma_{nf}B^2 v}{\rho_{nf}} \tag{3}$$

$$u\frac{\partial T}{\partial x}+v\frac{\partial T}{\partial y}+w\frac{\partial T}{\partial z}=\frac{k_{nf}}{\left(\rho C_P\right)_{nf}}\frac{\partial^2 T}{\partial z^2}+\frac{16\sigma^* T_\infty^3}{3k^*\left(\rho C_P\right)_{nf}}\frac{\partial^2 T}{\partial z^2} \tag{4}$$

$$u\frac{\partial a_1}{\partial x}+v\frac{\partial a_1}{\partial y}+w\frac{\partial a_1}{\partial z}=D_A\frac{\partial^2 a_1}{\partial z^2}-k_1^* a_1 b_1^2 \tag{5}$$

$$u\frac{\partial b_1}{\partial x}+v\frac{\partial b_1}{\partial y}+w\frac{\partial b_1}{\partial z}=D_B\frac{\partial^2 b_1}{\partial z^2}+k_1^* a_1 b_1^2 \tag{6}$$

where $\sigma_{nf}=\sigma_f\left[1+\dfrac{3\left(\dfrac{\sigma_p}{\sigma_f}-1\right)\phi}{\left(\dfrac{\sigma_p}{\sigma_f}+2\right)-\left(\dfrac{\sigma_p}{\sigma_f}-1\right)\phi}\right]$

In the energy equation (4), the term $\dfrac{16\sigma^* T_\infty^3}{3k^*\left(\rho C_P\right)_f}\dfrac{\partial^2 T}{\partial z^2}$ is obtained by assuming the temperature variation within the flow as small and expanding T^4 in a Taylor series about T_∞ and ignoring higher order terms and using the resulting expression in the Rosseland radiative heat flux (Brewster, 1972) $q_r=-\dfrac{4\sigma^*}{3k^*}\dfrac{\partial T^4}{\partial z}$.

The boundary conditions read:

$$\left.\begin{aligned} u=U_w=U_0\,exp\left[\frac{x+y}{L}\right], v=V_w=V_0\,exp\left[\frac{x+y}{L}\right],\ w=0,\\ -k_f\frac{\partial T}{\partial z}=h_f(T_f-T), D_A\left(\frac{\partial a_1}{\partial z}\right)=k_1^* a_1,\ D_B\left(\frac{\partial b_1}{\partial z}\right)=-k_2^* a_1\ \ at\ z=0\\ u\to 0, v\to 0, T\to T_\infty,\ a_1\to a_0, b_1\to 0\ \ as\ z\to\infty \end{aligned}\right\} \tag{7}$$

where u, v and w are velocity components along the *x*, *y* and *z*-directions, respectively, υ_f is the kinematic viscosity, T_∞ is the free stream temperature, σ is the electrical conductivity, B_0 is the maximum strength of variable magnetic field, ρ_f is the fluid density, U_0, V_0, U_w and V_w are constant velocities, L is the reference length, k_f is the thermal conductivity, h_f is the convective heat transfer coefficient, T_f is the temperature of the fluid heating the surface of the sheet, σ^* and k^* are respectively the Stefan-Boltzmann constant, and mean absorption coefficient. The effective

density of the nanofluid h_f and the heat capacitance of the nanofluids $\left(\rho C_p\right)_{nf}$ are defined in (Pak & Cho, 1998; Nayak et al., 2017; Pourmehran et al., 2016) as

$$\left.\begin{aligned}\rho_{nf} &= (1-\phi)\,\rho_f + \phi\rho_s \\ (\rho C_p)_{nf} &= (1-\phi)(\rho C_p)_f + \phi(\rho C_p)_s\end{aligned}\right\} \tag{8}$$

where $\left(\rho C_p\right)_f$ and $\left(\rho C_p\right)_s$ are respectively the heat capacitances of the base fluid and the nanoparticles, ρ_s and ρ_f are the densities of the pure fluid and the nanopartricles, respectively.

The effective dynamic viscosity of the nanofluid is described in (Pak & Cho, 1998; Nayak et al., 2017; Pourmehran et al., 2016) as

$$\mu_{nf} = \mu_f\left(1+39.11\phi+533.9\phi^2\right) \tag{9}$$

where μ_{nf} and μ_f are the effective dynamic viscosities of the nanofluid and the base fluid respectively, and ϕ is the solid volume fraction of nanoparticles.

Following the micro-convection model proposed by (Patel et al., 2005), the effective thermal conductivity of the nanofluid can be determined as

$$\left.\begin{aligned}\frac{k_{nf}}{k_f} &= 1+\frac{k_s A_s}{k_f A_f}+ck_s P_e\frac{A_s}{k_f A_f} \\ \frac{A_s}{A_f} &= \frac{d_f}{d_s}\frac{\phi}{1-\phi} \\ Pe = \frac{u_s d_s}{\alpha_f}, u_s &= \frac{2k_B T}{\pi\mu_f d_s^2}, c = 25,000\end{aligned}\right\} \tag{10}$$

where k_{nf}, k_f and k_s are respectively the thermal conductivities of the nanofluid, base fluid and the nanoparticles, A_s and A_f are the heat transfer area corresponding to particles and fluid media, respectively, $c(>0)$ is a constant, Pe is the Peclet number, d_f is the molecular size of the fluid and d_s is the nanoparticle diameter, u_s is the Brownian motion velocity, α_f is the thermal diffusivity of the fluid, and μ_f is the dynamic viscosity of the fluid.

In order to facilitate the analysis, we need the transformations:

$$\left.\begin{aligned} u = U_0\, exp\left[\frac{x+y}{L}\right]F'(\eta), v = U_0\, exp\left[\frac{x+y}{L}\right]G'(\eta), \\ w = -\sqrt{\frac{\upsilon_f U_0}{2L}}\, exp\left[\frac{x+y}{2L}\right]\left[F(\eta)+\eta F'(\eta)+G(\eta)+\eta G'(\eta)\right], \\ \theta(\eta) = \frac{T-T_\infty}{T_f-T_\infty}, G(\eta) = \frac{a_1}{a_0}, H(\eta) = \frac{b_1}{a_0}, \\ \eta = \sqrt{\frac{U_0}{2\upsilon_f L}}\, exp\left[\frac{x+y}{2L}\right]z \end{aligned}\right\} \tag{11}$$

Indeed, the diffusion coefficient of chemical species A and B are of a comparable size. In consideration of this, we assume that the diffusion coefficients D_A and D_B are equal, i.e., Ω=1(Chaudhary and Merkin, 1995).

This assumptions yields the relation

$$G(\eta)+H(\eta)=1 \tag{12}$$

Using Eqs. (9), (10), (11) and (12), Eqs. (2-5) and eq. (7) take the form

$$\phi_1 F''' + (F+G)F'' - 2(F'+G')F' - \left(\frac{\sigma_{nf}}{\sigma_f}\right)\phi_2 MF' = 0 \tag{13}$$

$$\phi_1 G''' + (F+G)G'' - 2(F'+G')G' - -\left(\frac{\sigma_{nf}}{\sigma_f}\right)\phi_2 MG' = 0 \tag{14}$$

$$\frac{1}{\Pr}\left(\phi_3 + \frac{4}{3}\phi_4 Rd\right)\theta'' + (F+G)\theta' = 0 \tag{15}$$

$$\frac{1}{Sc}G'' + FG' + GG' - \Gamma G(1-G)^2 = 0 \tag{16}$$

$$\left.\begin{aligned} F=0, G=0, F'=1, G'=\beta, \theta'(0) = -B_i\left[1-\theta(0)\right], G'(0) = \Gamma_1 G(0)\ at\ \eta=0 \\ F'\to 0, G'\to 0, \theta\to 0, G\to 1 \qquad as\ \ \eta\to\infty \end{aligned}\right\} \tag{17}$$

Where $\sigma_{nf} = \sigma_f\left[1 + \dfrac{3\left(\frac{\sigma_p}{\sigma_f}-1\right)\phi}{\left(\frac{\sigma_p}{\sigma_f}+2\right)-\left(\frac{\sigma_p}{\sigma_f}-1\right)\phi}\right]$

and

$$\left.\begin{aligned} M=\frac{2\sigma B_0^2 L}{\rho_f U_0},\beta=\frac{V_0}{U_0},P_r=\frac{\upsilon_f}{\alpha_f},Rd=\frac{4\sigma^* T_\infty^3}{3k_f k^*},\\ Bi=\frac{\varepsilon}{k_f\sqrt{\frac{U_0}{2\upsilon_f L}}},\varepsilon=\frac{h_f}{exp\left(\frac{x+y}{2L}\right)},\Gamma=\frac{2k_1^* a_0^2 L}{U_w},\Gamma_1=\frac{k_1^*\sqrt{2\upsilon L/U_w}}{D_A} \end{aligned}\right\} \tag{18}$$

Here $M,\beta,\Pr,R_d$, Bi, Γ and Γ_1 are respectively is the Hartmann number, ratio parameter, Prandtl number, thermal radiation parameter, Biot's number, homogenous reaction strength parameter and heterogeneous reaction strength parameter. The nanoparticle volume fraction constants $\phi_i(i=1,2,3,4)$ are defined as

$$\phi_1=\frac{\nu_{nf}}{\nu_f}=\frac{1+39.11\phi+533.9\phi^2}{1-\phi+\phi(\rho_s/\rho_f)},\ \phi_2=\frac{\rho_f}{\rho_{nf}}=\frac{1}{1-\phi+\phi(\rho_s/\rho_f)},$$

$$\phi_3=\frac{1+\frac{k_s}{k_f}\frac{d_f}{d_s}\left(\frac{\phi}{1-\phi}\right)+c\frac{k_s}{k_f}Pe\left(\frac{\phi}{1-\phi}\right)}{1-\phi+\phi[(\rho C_p)_s/(\rho C_p)_f)},\ \phi_4=\frac{1}{1-\phi+\phi[(\rho C_p)_s/(\rho C_p)_f)},$$

The skin friction coefficients along axial and transverse directions are:

$$C_{fx}=\frac{\tau_{wx}}{\left(\frac{1}{2}\right)\rho_f U_w^2} \tag{19}$$

$$C_{fy}=\frac{\tau_{wy}}{\left(\frac{1}{2}\right)\rho_f V_w^2} \tag{20}$$

where τ_{wx} and τ_{wy} are the wall shear stresses.

The dimensionless form of the skin friction coefficient along axial and transverse directions are obtained respectively as

$$\left(\frac{\mathrm{Re}_x}{2}\right)^{\frac{1}{2}}C_{fx}=\left(1+39.11\phi+533.9\phi^2\right)F''(0) \tag{21}$$

$$\left(\frac{\mathrm{Re}_y}{2}\right)^{\frac{1}{2}}C_{fy}=\left(1+39.11\phi+533.9\phi^2\right)G''(0) \tag{22}$$

The local Nusselt number,

$$Nu_x=\frac{xq_w}{k_f\left(T_w-T_\infty\right)} \tag{23}$$

where q_w is the wall heat flux.

The dimensionless local Nusselt number is

$$\left(\frac{\mathrm{Re}_x}{2}\right)^{-1/2} Nu_x = -\left(\frac{k_{nf}}{k_f} + Rd\right)\frac{x}{L}\theta'(0) \tag{24}$$

Where $\mathrm{Re}_x = \frac{U_w L}{\upsilon_f}$ and $\mathrm{Re}_y = \frac{V_w L}{\upsilon_f}$ are the local Reynolds numbers.

3. Results and Discussion

The present study provides an all-round emphasis on the behavior of homogenous and heterogeneous reactions, variable magnetic field and thermal radiation on three-dimensional nanofluid flows past an exponentially-stretching sheet. Specifically, the Patel et al., 2005 model is applied for an appreciable enhancement of the thermal conductivity and hence, the heat transfer capability of nanofluids. Furthermore, a convective heat transfer model is employed where the bottom surface of the plate gets heated from a hot fluid of temperature T_f providing a heat transfer coefficient h_f. The solutions of the transformed boundary layer equations have been devised using fourth-order Runge-Kutta method along with shooting method. In the present analysis, we deem three different kinds of base fluids such as water, water with 30% ethylene glycol, water with 50% ethylene glycol and three nanoparticles such as Cu (copper), Ag (silver) and Al_2O_3 (alumina). The thermophysical properties of both the base fluids and the nanoparticles are incorporated in Table 1. To get the accuracy, the results obtained in the present study are compared and validated in Table 2 with the noteworthy works of Nadeem et al., 2014; Magyari and Keller, 1999 and Liu et al., 2013. These comparisons as well as the validation confirm that our numerical results are found to be agreed well for all considered values of parameters and therefore, we are confident about the accuracy and generality of our results.

To begin with Figs. 2 and 3 portray the developed variation of the velocity profiles along the axial and transverse directions for different values of the Hartmann number *M*. We have understood from these figures that both the axial and transverse velocities decline due to the enhancement of the Hartmann number leading to a thinner momentum boundary layer. This is obvious due to the reason that the electromagnetic interaction between the magnetic field and electrically-conducting fluid establishes a retarding Lorentz force that impedes the fluid motion in the entire boundary layer region. The most fascinating aspect of this observation is that the deceleration of velocity is significant for relatively higher values of the Hartmann number. This result is in good agreement with the results of Mabood et al., 2016.

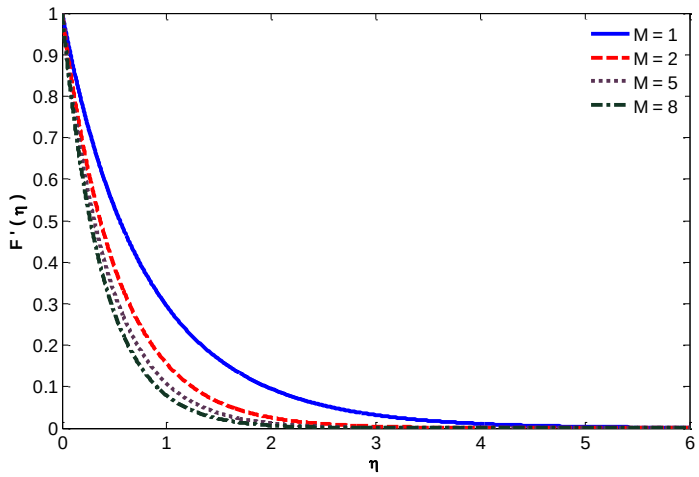

Fig.2 Axial velocity profiles for different Hartman number (pure water, Cu nanoparticles)

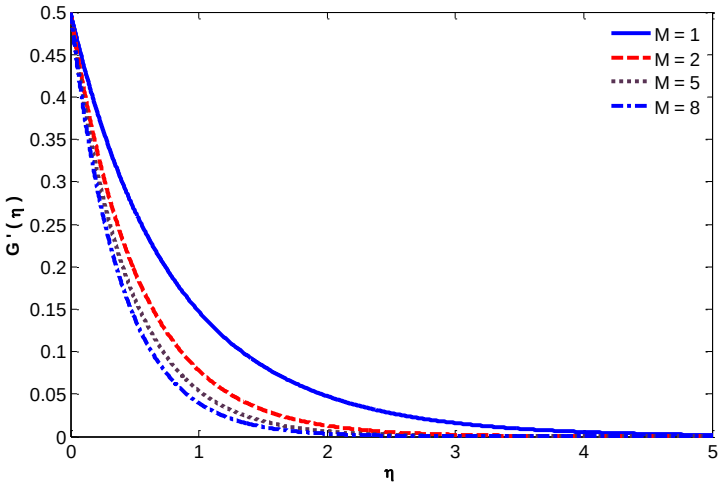

Fig. 3 Transverse velocity profiles for different Hartman number (pure water, Cu nanoparticles)

Fig. 4 addressed the behavior of the non-dimensional temperature profiles under the influence of the Hartmann number M. The important outcome has been accomplished from this sighting is that a higher value of M enables the non-dimensional temperature to rise as is observed earlier in Nadeem et al., 2014. The only basic reason for this enhancement is that an increase in the Hartmann number generates electromagnetic force in greater strength that restrains the fluid motion which in turn produces more heat that causes the temperature rise. As a consequence, thicker thermal boundary layer is accomplished. In fact, had there been no magnetic field, the temperature could not be enhanced in the flow field. An interesting consequence of the temperature profiles due to the presence of magnetic field is that the rise in the fluid temperature is significant for relatively higher values of the Hartmann number M.

Physically, the Prandtl number is nothing but the ratio of the kinematic viscosity to the thermal diffusivity. We express this influence by saying that a higher Prandtl fluid such as ethylene glycol (30% with $\mathrm{Pr} = 13.5$ and 50%with $\mathrm{Pr} = 24.4$) having a lower thermal diffusivity yields a

reduction in the fluid temperature in association with shrinkage of thermal boundary layer. On the other hand, the reverse effect is attained for a lower Prandtl fluid such as water $(\mathrm{Pr}=7)$ as illustrated in Fig.5. In other words, an increase in the Prandtl number enhances the heat transfer rate at the surface as the temperature gradient at the surface gets enhanced (Nayak, 2017).

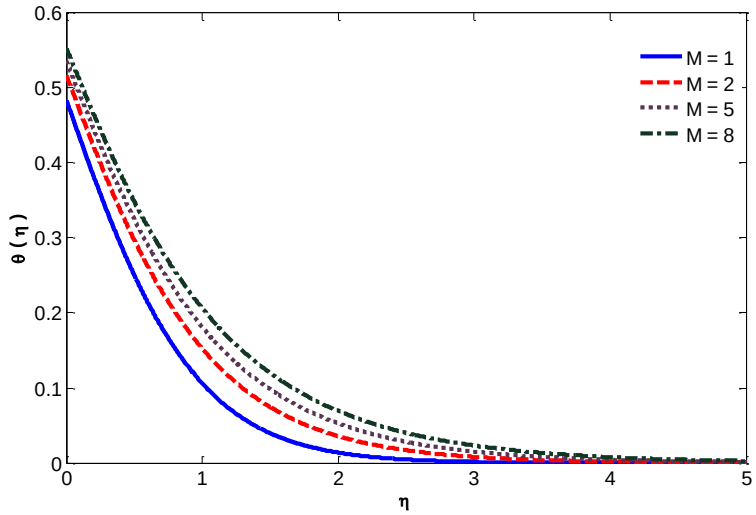

Fig.4 Temperature profiles for different Hartman number (pure water, Cu nanoparticles)

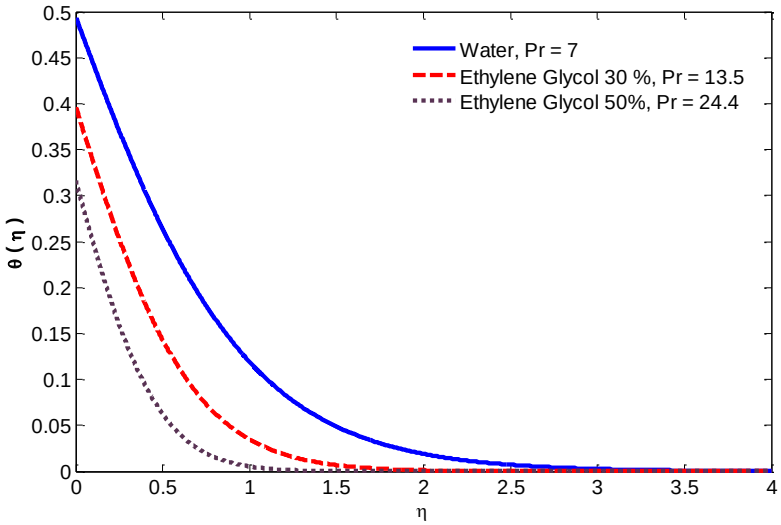

Fig. 5 Temperature profiles for different Prandtl number (Cu nanoparticles)

A significant impact of radiation effect on the non-dimensional temperature is displayed in Fig.6. It focuses that the non-dimensional fluid temperature increases due to an increase in the radiation parameter leading to a growth of the thermal boundary layer. As a result more heat will transfer from the sheet into the fluid thereby producing more cooling (Nayak, 2016).

The characteristics of the axial velocity, transverse velocity and the temperature profiles for different nanoparticles volume fraction ϕ are revealed from Figs.7 – 9. From these illustrations,

it follows that the axial as well as the transverse velocities and the related velocity boundary layer thickness get enhanced due to an increase in ϕ while the opposite trend prevails for the fluid temperature indicating a narrowing of the thermal boundary layer (Mabood et al., 2016).

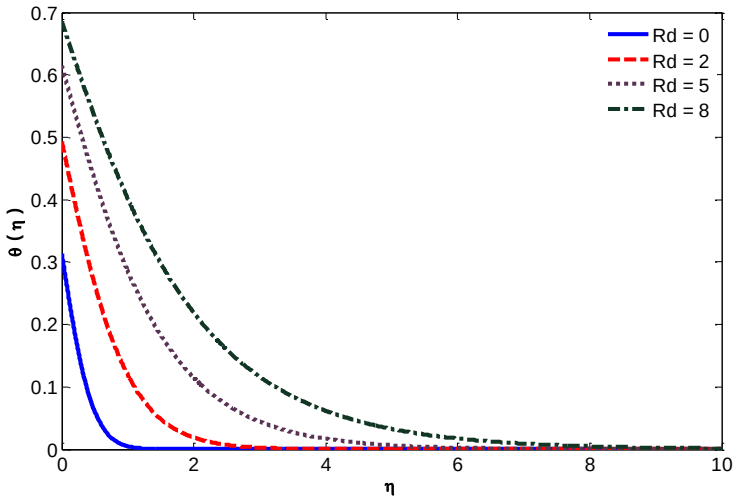

Fig. 6 Temperature profiles for different radiation parameter (Cu nanoparticles)

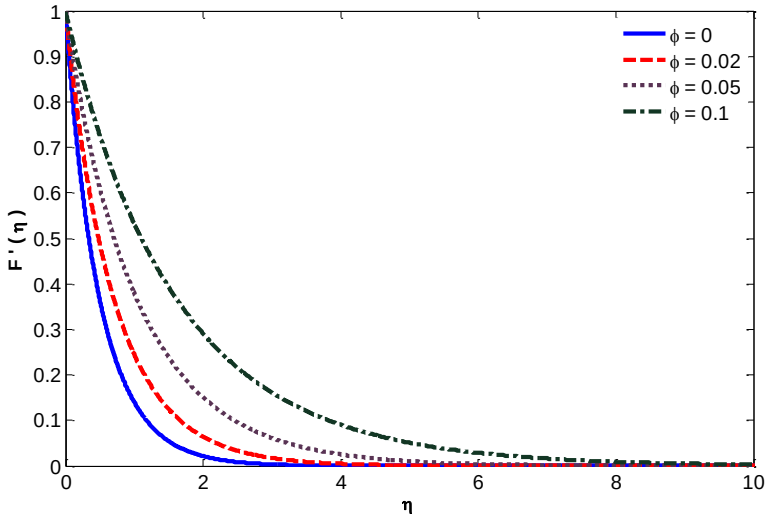

Fig. 7 Axial velocity profiles for different volume fraction (pure water, Cu nanoparticles)

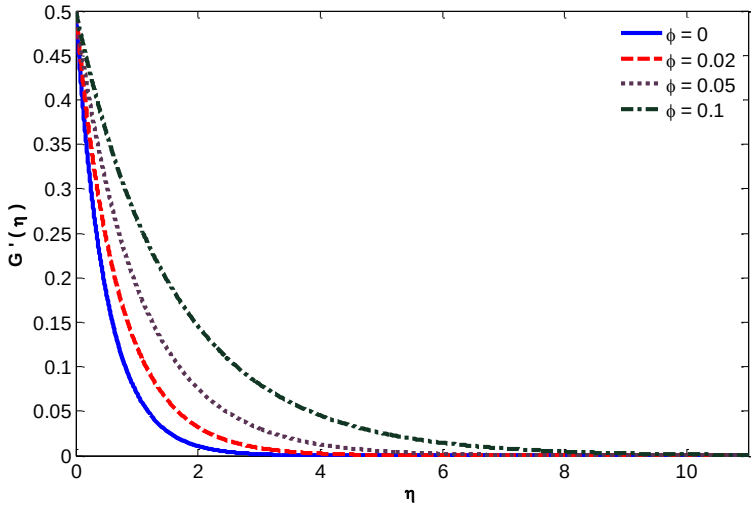

Fig. 8 Transverse velocity profiles for different volume fraction (pure water, Cu nanoparticles)

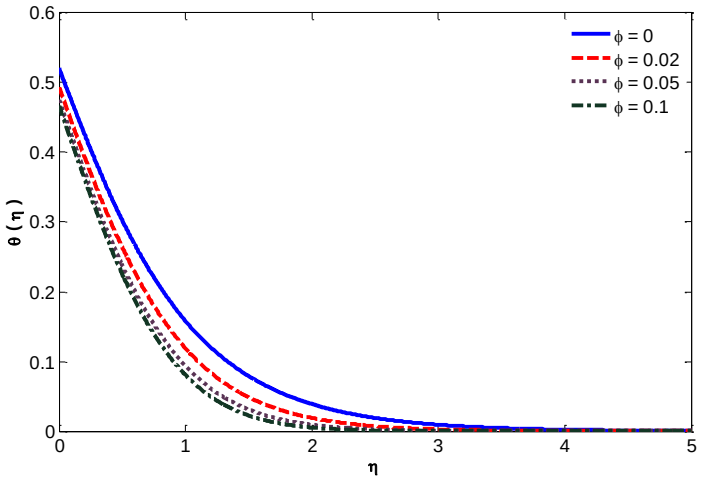

Fig. 9 Temperature profiles for different volume fraction (pure water, Cu nanoparticles)

From Fig.10 it is envisaged that the non-dimensional temperature and hence, the thermal resistance increases due to an enhancement in the Biot number Bi. However, the increase in temperature is significant for higher Bi values. The variations of the non-dimensional velocities (axial as well as transverse) and the non-dimensional temperature of the fluid in response to different values of the stretching ratio are made known from Figs.11-13. Actually, the stretching ratio is the ratio between the transverse and axial velocities of the stretching sheet. An increase in the stretching ratio means that the transverse velocity becomes larger than the axial velocity. Considering the above concept in mind and observing from the Figs.11 and 12 that the axial velocity decreases due to an increase in the stretching ratio parameter β while the transverse velocity shows the opposite trend. However, it must be noted from Fig.13 that the non-dimensional temperature (and hence, the thermal resistance of the fluid) and the thermal boundary layer thickness get diminution due to an increase in the stretching ratio parameter (Ibrahim et al., 2013).

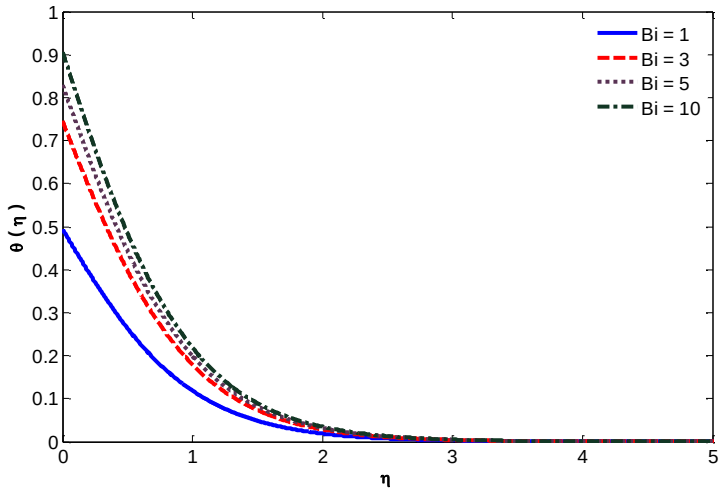

Fig.10 Temperature profiles for different Biot number (pure water, Cu nanoparticles)

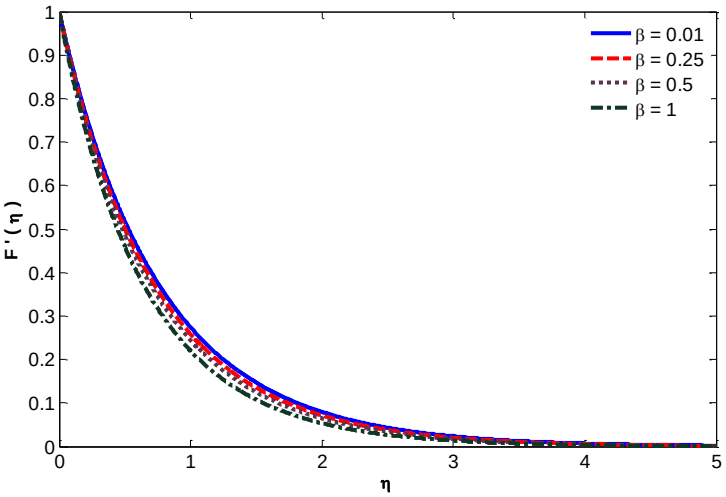

Fig.11 Axial velocity profiles for different ratio parameter (pure water, Cu nanoparticles)

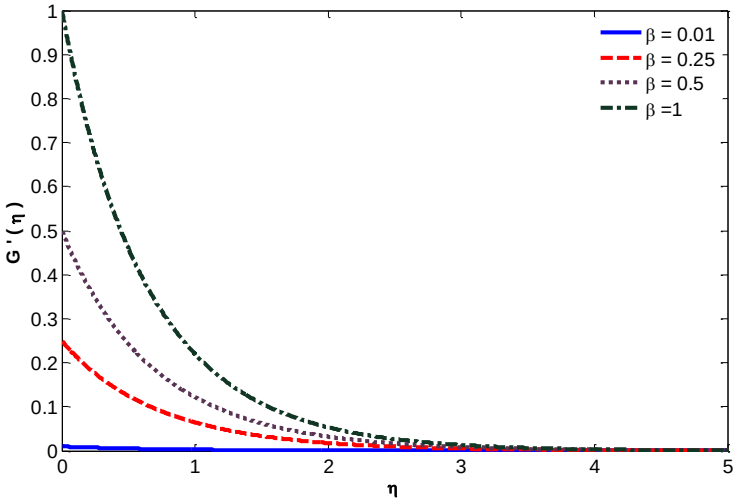

Fig.12 Transverse velocity profiles for different ratio parameter (pure water, Cu nanoparticles)

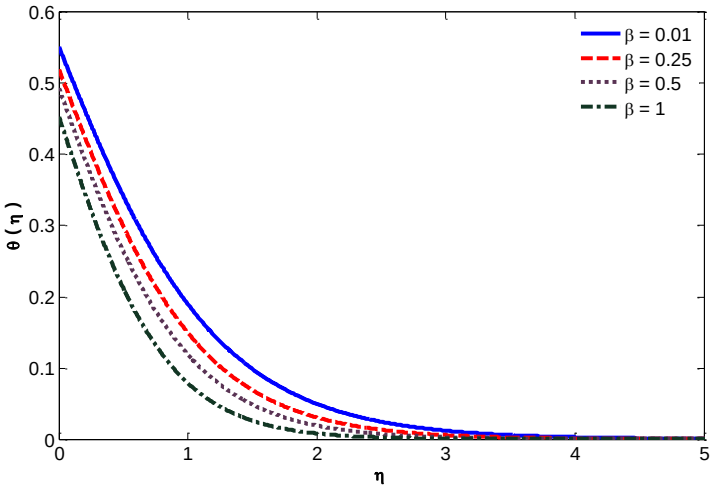

Fig.13 Temperature profiles for different ratio parameter (pure water, Cu nanoparticles)

It has been acknowledged from Fig.14 that increase in Schmidt number Sc contributes to upsurge in concentration and the related concentration boundary layer. Fig.15 points out that rising values of Γ peter out nanoparticle concentration yielding reduction in wall concentration gradient. It well agrees with Mabood et al. [2016]. It would be much more remarkable to visualize Fig. 16 where the fluid concentration belittles faster in response to lower value of Γ_1 and slower with higher value of it.

While it is most certain that Figs.17 and 18 disclose the behavior of the axial as well as the transverse skin friction with the nanoparticles volume fraction for different Hartmann number *M*. It is well understood from this figure that the axial as well as the transverse skin friction undermine due to an increase in the value of M for pure water as the base fluid with Cu nanoparticles. In other words, an increase in the magnetic field strength causes reduction in the axial as well as the transverse wall shear stresses in the entire flow domain.

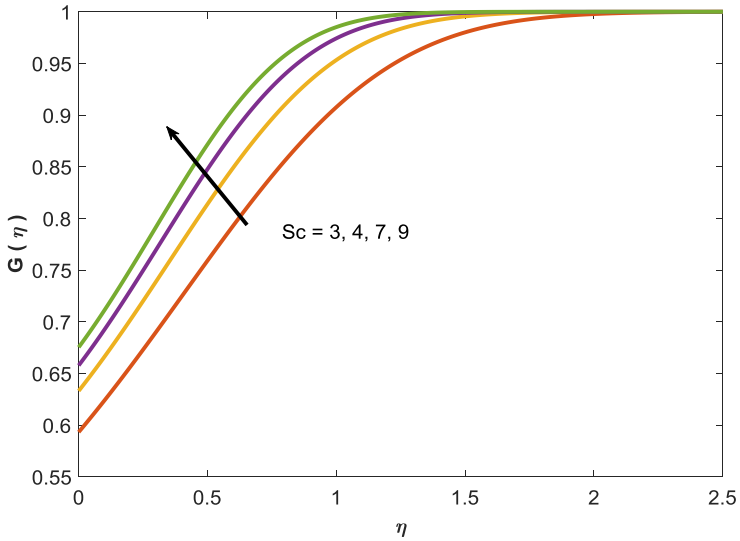

Fig.14 Concentration profile for different Schmidt number Sc.

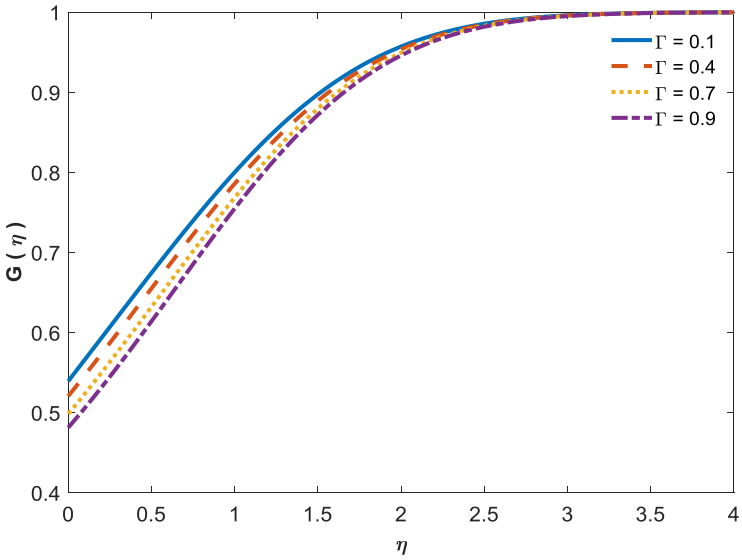

Fig.15 Concentration profile for different strength of the homogeneous reaction parameter Γ .

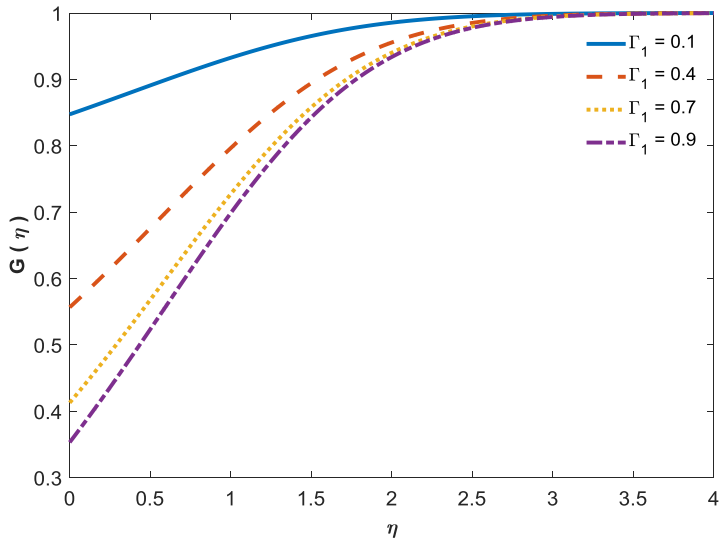

Fig.16 Concentration profile for different strength of the heterogeneous reaction parameter Γ_1

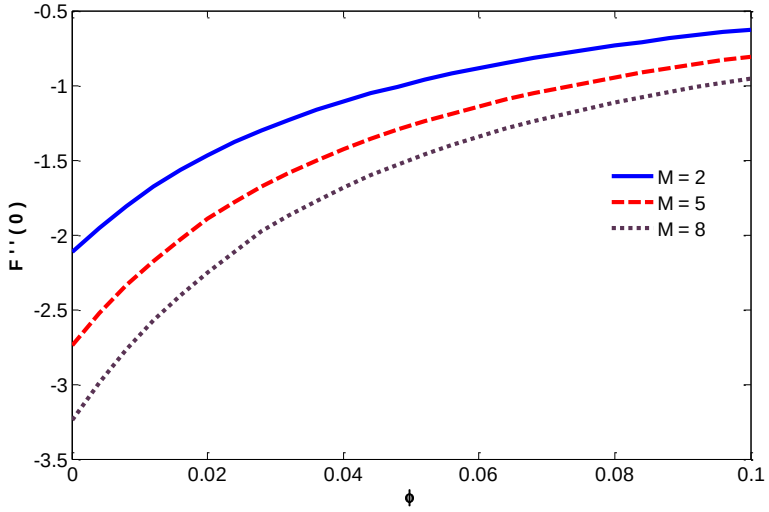

Fig. 17 Axial skin friction in response to volume fraction for different Hartman number (pure water, Cu nanoparticles)

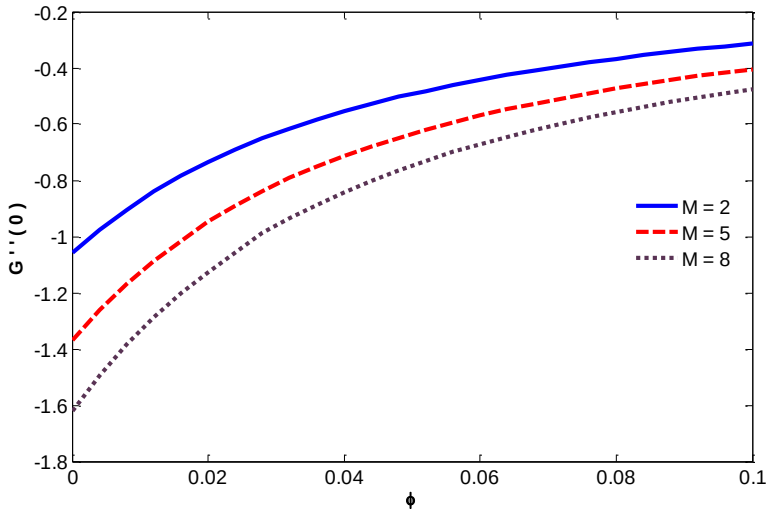

Fig. 18 Transverse skin friction in response to volume fraction for different Hartman number (pure water, Cu nanoparticles)

The variation of the reduced Nusselt number $-\theta'(0)$ with the increase in the Hartmann number M affiliated with the nanoparticles volume fraction is seen in Fig. 19. One must acknowledge here that the increase in the magnetic field strength upsurges the thermal resistance thereby enhancing the fluid temperature which in turn reduces the heat transfer rate from the surface indicating less cooling.

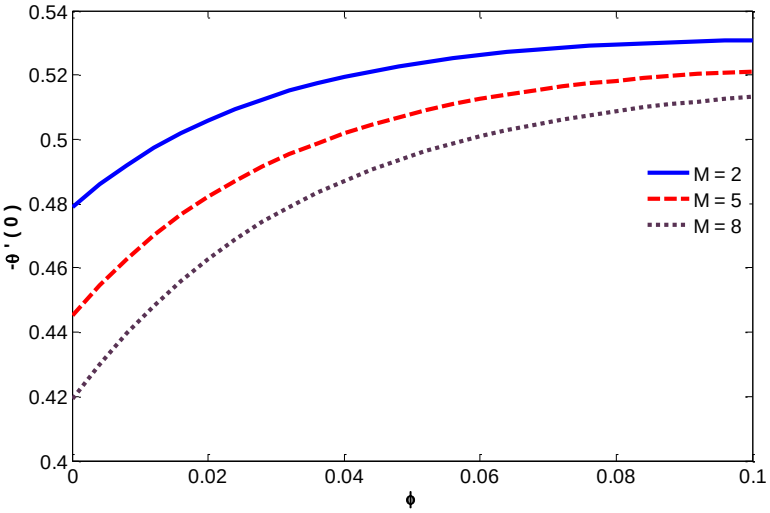

Fig. 19. LocalNusselt number in response to volume fraction for different magnetic parameter (pure water, Cu nanoparticles)

Table 2 provides comparisons of the present results with the results published earlier by noteworthy researchers (Nadeem et al., 2014; Magyari and Keller, 1999; Liu et al., 2013) available in the literature. In these comparisons, we find that an increase in the Prandtl number Pr for a pure fluid decreases the thermal resistance thereby increasing the heat transfer rate. This result is well-agreed with Nadeem et al., 2014; Magyari and Keller, 1999 and Liu et al., 2013.

From the data incorporated in Table 3, it is obvious that prior to the strength of magnetic field, an increase in the Hartmann number M decreases the axial as well as the transverse skin frictions for all nanoparticles such as Ag, Cu and Al_2O_3. However, at a fixed value of M, the axial and transverse skin frictions (absolute values) increase in the order of choice of nanoparticles viz. Ag, Cu and Al_2O_3. We say that an increase in the Hartmann number M disparages the heat transfer rate. There is a good, valid and compelling reason for such diminution of the local skin frictions as well as hike of the wall temperature gradient that the retarding Lorentz force restrains the fluid motion from its pristine condition and boosts the strength of the thermal resistance thereby enhancing the non-dimensional fluid temperature. Another point to be noted is that at fixed value of M, the heat transfer rate gets enhanced in the order of nanoparticles Ag, Cu and Al_2O_3 indicating more cooling from the surface.

It is pertinent that an increase in the thermal radiation enhances the heat transfer rate from the surface for all nanoparticles viz. Ag, Cu and Al_2O_3. Notwithstanding, the nanoparticles types like Ag, Cu and Al_2O_3, an increase in the ratio parameter β decreases the axial as well as the transverse wall shear stresses whereas the influence of β attains a reverse trend on the heat transfer rate. One can say that there is an increase in the wall temperature gradient due to the Biot number Bi for all nanoparticles. Let us discuss in a little more detail the impact of nanoparticles volume fraction ϕ on the local skin frictions and the rate of heat transfer. It has been traced that the axial as well as the transverse skin frictions (or wall shear stresses) and the heat transfer rate get enhanced due to an increase in the value of ϕ.

Table1 Thermo-physical properties of the base fluid and nanoparticles at T=300 K.

	$\rho\ (Kg/m^3)$	$C_P\ (J/Kg\ K)$	$k\ (W/m\ K)$	$\mu_f\ (N\ s/m^2)$	$d_f\ or\ d_s(nm)$
Pure Water	997.1	4179	0.613	0.001003	0.24
Ethylene glycol 30%	1034	3736.2	0.489	0.0017613	0.45
Ethylene glycol 50%	1052.1	3301.7	0.432		30-60
Copper (Cu)	8933	385	401		30-60
Silver (Ag)	10500	2235	429		30-60
Alumina (Al_2O_3)	3970	765	40		30-60

Table 2 Comparison with the literature of heat transfer rate for pure fluid M=0, A=0, β =0 results with Nadeem et al., 2014; Magyari and Keller, 1999 and Liu et al., 2013.

Pr	Magyari and Keller, 1999	Liu et al., 2013	Nadeem et al., 2014	Present
0.7		-0.4258380	-0.42584	-0.42583456
1	-0.549643	-0.54964375	- 0.549646	-0.54964072
5	-1.521243	-1.52123900	-1.521240	-1.52121586
7		-1.8466056	-1.84661	
10	-2.257429	-2.25742372	-2.257424	--2.25737274

Table 3 Skin frictions $F''(0)$ and $G''(0)$ and local Nusselt number $-\theta'(0)$ for different $\phi, A, \beta, \lambda_T, M, Bi$ with $\Pr = 7$.

ϕ	Bi	β	Rd	M	$F''(0)$	$G''(0)$	$-\theta'(0)$
0.02	1	0.5	2	2	-1.49379940 (Cu)	-0.74689970 (Cu)	0.50598557 (Cu)
					-1.49696035 (Al_2O_3)	-0.74848018 (Al_2O_3)	0.50814768 (Al_2O_3)
					-1.49254979 (Ag)	-0.74627490 (Ag)	0.50508328 (Ag)
	10				-1.49379940 (Cu)	-0.74689970 (Cu)	0.92907363 (Cu)
					-1.49696035 (Al_2O_3)	-0.74848018 (Al_2O_3)	0.93638936 (Al_2O_3)
					-1.49254979 (Ag)	-0.74627490 (Ag)	0.92603608 (Ag)
	1	0.75			-1.56062742 (Cu)	-1.17047057 (Cu)	0.52781722 (Cu)
					-1.56415506 (Al_2O_3)	-1.17311629 (Al_2O_3)	0.52994638 (Al_2O_3)
					-1.55923271 (Ag)	-1.16942453 (Ag)	0.52692839 (Ag)
		0.5	5		-1.49379940 (Cu)	-0.74689970 (Cu)	0.38444316 (Cu)
					-1.49696035 (Al_2O_3)	-0.74848018 (Al_2O_3)	0.38524039 (Al_2O_3)
					-1.49254979 (Ag)	-0.74627490 (Ag)	0.38362390 (Ag)
			2	5	-1.93342640 (Cu)	-0.96671320 (Cu)	0.48225584 (Cu)
					-1.93587858 (Al_2O_3)	-0.96793929 (Al_2O_3)	0.48463949 (Al_2O_3)
					-0.77725136 (Ag)	-0.35353036 (Ag)	1.46714265 (Ag)
0.05				2	-1.01360975 (Cu)	-0.50680487 (Cu)	0.52388398 (Cu)
					-1.01901889 (Al_2O_3)	-0.50950944 (Al_2O_3)	0.52903285 (Al_2O_3)
					-1.01146649 (Ag)	-0.50573325 (Ag)	0.52175609 (Ag)

4. Conclusion

The present analysis squares up with the effects of homogenous and heterogeneous reactions; variable magnetic field and thermal radiation associated with the significant governing parameters on the flow of an electrically-conducting incompressible nanofluid over an exponentially-stretching sheet subject to convective boundary condition through appreciable discussion with the help of graphs and tables. The numerical results accomplished here are in conformity with the previous results published by (Nadeem et al., 2014; Magyari and Keller, 1999; Liu et al., 2013).

The major concluding remarks according to the state of the art of the present study are:

1. Presence of magnetic field develops a restraining Lorentz force that impedes the fluid motion along the axial as well as the transverse directions leading to a thinner velocity boundary layer while it enhances the thermal resistance enhancing thermal boundary thickness.

2. Augmented homogenous parameter Γ belittles the concentration and the related concentration boundary layer.

3. Enhanced heterogeneous parameter Γ_1 declines the wall concentration gradient.

References

Alsabery, A., Chamkha, A.J. and Hashim, I. (2016). Heat line visualization of conjugate natural convection in a square cavity filled with nanofluid with sinusoidal temperature variations on both horizontal walls. *Int. J. Heat Mass Transfer*, 100, 835-850.

Aziz, A. (2009). A similarity solution for laminar thermal boundary layer over a flat plate with a convective surface boundary condition. *Comm. Nonlinear Sci. Num. Simul*., 14(4), 1064-1068.

Brewster, M.Q. (1972). Thermal radiative transfer properties. *Wiley*, New York.

Choi, S.U.S. (1995). Enhancing thermal conductivity of fluids with nanoparticles. *ASME Fluids Eng. Division* 231, 99–105.

Hayat, T., Shafique, M., Tanveer, A. and Alsaedi, A. (2016). Magnetohydrodynamic effects on peristaltic flow of hyperbolic tangent nanofluid with slip conditions and Joule heating in an inclined channel. *Int. J. Heat Mass Transf*. 102, 54–63.

Ibrahim, W., Shankar, B. and Nandeppanavar, M.M. (2013). MHD stagnation point flow and heat transfer due to nanofluid towards a stretching sheet. *Int. J. Heat Mass Transf*. 56, 1-9.

Ishak, A. (2010). Similarity solutions for flow and heat transfer over a permeable surface with convective boundary condition. *Appl. Math. Comp*., 217(2), 837-842.

Ismael, M.A., Mansour, M.A., Chamkha, A.J. and Rashad, A.M. (2016). Mixed convection in a nanofluid filled-cavity with partial slip subjected to constant heat flux and inclined magnetic field. *J. Magn. Magn.Mater*. 416, 25–36.

Khan, W. and Pop, I. (2010). Boundary-layer flow of a nanofluid past a stretching sheet. *Int. J. Heat Mass Transfer*, 53, 2477-2483.

Liu, C., Wang, Hung-H. and Peng, Yih-F. (2013). Flow and heat transfer for three-dimensional flow over an exponentially stretching surface. *Chemical Eng. Com*. 200, 253–268.

Mabood, F., Shateyi, S., Rashidi, M.M., Momoniat, E. and Freidoonimehr, N. (2016). MHD stagnation point flow heat and mass transfer of nanofluids in porous medium with radiation, viscous dissipation and chemical reaction. *Adv. Powder Technol*. 27, 742-749.

Magyari, E. and Keller, B. (1999). Heat and mass transfer in the boundary layers on an exponentially stretching continuous surface, *J. Phy. D. Appl. Phy*. 32, 577–585.

Makinde, O.D. and Aziz, A. (2011). Boundary layer flow of a nanofluid past a stretching sheet with a convective boundary condition. *Int. J. Ther. Sci*., 50, 1326-1332.

Makinde, O.D. and Ogulu, A. (2008). The effect of thermal radiation on the heat and mass transfer flow of a variable viscosity fluid past a vertical porous plate permeated by a transverse magnetic field. *Chem. Eng. Commn*. 195(12), 1575–1584.

Makinde, O.D. and Animasaun, I.L. (2016). Bioconvection in MHD nanofluid flow with nonlinear thermal radiation and quartic autocatalysis chemical reaction past an upper surface of a paraboloid of revolution. *Int. J. Ther. Science*, 109, 159-171.

Nadeem, S., Haq, R.Ul. and Khan, Z.H. (2014). Heat transfer analysis of water-based nanofluid over an exponentially stretching sheet, *Alex. Eng. J.* 53(1), 219–224.

Nayak, M.K., Dash, G.C. and Singh, L.P. (2015). Unsteady radiative MHD free convective flow and mass transfer of a viscoelastic fluid past an inclined porous plate. *Arab. J. Sci. Eng*., 40, 3029-3039.

Nayak, M.K. (2016). Chemical reaction effect on MHD viscoelastic fluid over a stretching sheet through porous medium, *Meccanica*, 51, 1699-1711.

Nayak, M.K., Dash, G.C. and Singh, L.P. (2014). Steady MHD flow and heat transfer of a third grade fluid in wire coating analysis with temperature dependent viscosity. *Int. J. Heat Mass Transf.* 79, 1087–1095.

Nayak, M.K., Akbar, N.S., Pandey, V.S., Khan, Z.H. and Tripathi, D. (2017). 3D free convective MHD flow of nanofluid over permeable linear stretching sheet with thermal radiation, *Powder Technol.* 315, 205-215.

Nayak, M.K, Akbar, N.S., Pandey, V.S., Khan, Z. H., Tripathi,D. (2017). MHD 3D free convective flow of nanofluid over an exponential stretching sheet with chemical reaction. *Adv. Powder Technol*. 28(9), 2159-2166.

Nayak, M.K, Akbar, N.S., Pandey, V.S., Tripathi,D. (2017). Three dimensional MHD flow of nanofluid over an exponential stretching sheet with convective boundary conditions, *Thermal Sci. Eng. Progress*, 3, 133-140.

Nayak, M.K. (2017). MHD 3D flow and heat transfer analysis of nanofluid by shrinking surface inspired by thermal radiation and viscous dissipation. *Int. J. Mech. Sci*. 124, 185-193.

Nayak, M K, Shaw, S, Chamkha, A J, (2018). Radiative non linear heat transfer analysis on wire coating from a bath of third-grade fluid, *Thermal Sci. Eng. Progress*, 5, 97-106.

Nayak, M K, Shaw, S, Pandey, V S, Chamkha, A.J., (2018). Combined effects of slip and convective boundary condition on MHD 3D stretched flow of nanofluid through porous media inspired by non-linear thermal radiation, *Indian J Phys*, DOI: 10.1007/s12648-018-1188-2.

Nayak, M. K., Shaw, S., Makinde, O. D., Chamkha, A.J.(2018). Effects of Homogenous–Heterogeneous reactions on radiative NaCl-CNP nanofluid flow past a convectively heated vertical Riga plate, *J. Nanofluids*, 7(4). DOI: 10.1166/jon.2018.1501.

Pandey, A.K. and Kumar, M. (2017). Natural convection and thermal radiation influence on nanofluid flow over a stretching cylinder in a porous medium with viscous dissipation. *Alexandria Eng. Journal*, 56, 55–62.

Pak, B.C. and Cho, Y.I. (1998). Hydromagnetic and heat transfer study of dispersed fluids with submicron metallic oxide particles. *Exp. Heat Transfer*, 11, 151-171.

Patel, H.E., Sundararajn, T., Pradeep, T., Dasgupta, A., Dasgupta N. and Das, S.K. (2005). A micro-convection model for thermal conductivity of nanofluids, *Pramana J. Physics*, 65(5), 863-869.

Pourmehran, O., Rahimi-Gorji, M. and Ganji, D.D. (2016). Heat transfer and flow analysis of nanofluid flow induced by a stretching sheet in the presence of an external magnetic field. *J. Taiwan Inst. Chem. Eng.* 65, 162-171.

Prasad, K. V., Vajravelu, K. Vaidya, H., Rashidi, M. M. and Basha, N.Z. (2018). Flow and Heat Transfer of a Casson Liquid over a Vertical Stretching Surface: Optimal Solution. *American J. Heat Mass Transfer,* 5 (1), 1-22.

Priyadarsan, K. P., Nayak, M. K., Panda, S. (2017). Heat transfer effects on MHD 3D flow of nanofluid by a shrinking surface. *American J. Heat Mass Transfer,* 4(2) 64-84.

Reddy, S. and Chamkha, A.J. (2016). Soret and Dufour effects on MHD convective flow of Al_2O_3-water and TiO_2-water nanofluids past a stretching sheet in porous media with heat generation/absorption. *Adv. Powder Technology*, 27, 1207-1218.

Sengupta, S. and Deb, R. (2018). MHD Free Convection Mass Transfer Flow of Radiative Micropolar Fluid with Soret Effect and Uniform Heat and Mass Fluxes. *American J. Heat Mass Transfer*, 5 (1), 49-75.

Sheikholeslami, M., Hatami, M. and Ganji, D.D. (2014). Nanofluid flow and heat transfer in a rotating system in the presence of a magnetic field. *J. Mol. Liq.* 190, 112-120.

Sheikholeslami, M. and Shehzad, S.A. (2017). Thermal radiation of ferrofluid in existence of Lorentz forces considering variable viscosity. *Int. J Heat Mass Trans*fer, 109, 82–92.

Sheikholeslami, M., Ellahi, R. and Vafai, K. (2017). Study of Fe3O4-water nanofluid with convective heat transfer in the presence of magnetic source. *Alexandria Eng. Journal*, DOI: org/10.1016/j.aej.2017.01.027.